I&EC research
Industrial & Engineering Chemistry Research

pubs.acs.org/IECR

Article

Mixing Efficiency and Residence Time Distributions of a Side-Injection Tubular Reactor Equipped with Static Mixers

Jody Albertazzi, Federico Florit, Valentina Busini,* and Renato Rota

Cite This: https://doi.org/10.1021/acs.iecr.1c00575

Read Online

ACCESS | Metrics & More | Article Recommendations

ABSTRACT: Plug flow behavior in tubular reactors is often highly desirable in industry, since it can ensure high productivity, good selectivity, and enhanced heat transfer. To achieve this, good radial mixing combined with poor axial mixing is required: these conditions are quite easy to obtain if the flow regime is turbulent, but they are much more challenging to achieve if the flow is laminar. In this work radial mixing and residence time distributions in a side-injected tubular reactor equipped with a series of Sulzer SMX static mixers were investigated using Computational Fluid Dynamics. It was found that even at low values of Reynolds number the reactor can efficiently satisfy the plug flow conditions, and operative diagrams were determined to foresee the reactor behavior.

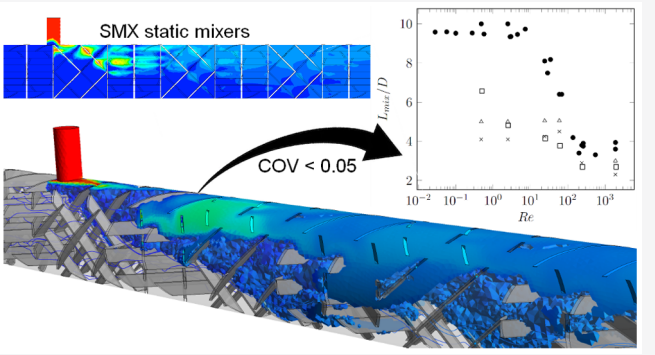

INTRODUCTION

Continuous and discontinuous processes represent the two production modes adopted in the chemical industry. In a batch process, raw materials are charged before the processing, and the products are discharged afterward. Instead, continuous reactors can be operated without any interruption for discharge and cleaning procedures. Normally, the fine chemical industry (polymers and pharmaceutical) prefers batch processes for their simplicity and their flexibility as multipurpose systems.[1,2] Nevertheless, in the past few years, there is a tendency to shift to continuous processes[3,4] which allow the gain of several advantages over discontinuous systems, such as reduced volumes, higher productivities, automatization with simpler control, and most importantly, constant quality of the produced chemicals.[5,6] Among continuous reactors, tubular reactors guarantee a better heat exchange than continuous stirred tank reactors (CSTRs) due to a higher heat transfer area-to-volume ratio. This characteristic allows tubular reactors to operate in more severe reaction conditions and to obtain a larger productivity, keeping the process safe and at a constant quality. This is generally the case when the tubular reactor operates as a plug-flow reactor (PFR). On the other hand, if the tubular reactor operates with extremely low flow rates (such as when a large reaction time is needed), a laminar flow can be attained in the reactor, leading to a wide distribution of reaction times in the reactor and an overall uneven distribution of chemicals. These conditions deviate from the desired PFR behavior and can lead to quality and safety issues.

PFRs are characterized by (i) complete radial mixing of the chemical species, meaning that no radial composition gradient is present, and (ii) no axial dispersion, meaning that axial concentration gradients are caused only by convection and reaction phenomena.

These conditions are easily satisfied for processes led in empty tubes that attain fully developed turbulent flow (which is attained for Reynolds number $Re > 4000$ in tubular reactors[7]), because the vortexes induced by turbulence tend to homogenize properties along the radial coordinate of the reactor, due to the turbulent diffusion process. On the other hand, turbulent flow requires large velocities, thus this solution can be adopted only for fast reactions which require small residence times in the reactor (which is usually not the case in the pharmaceutical and polymer industries). Instead, empty reactors in laminar regime have to rely on molecular diffusion to even out radial gradients.[8,9] Therefore, a plug-flow (PF) behavior can only be achieved in an empty tube if the reactor is extremely long[9,10] or if the tube is bent or coiled to reduce axial dispersion.[11,12] Alternatively, the process can be carried out in a series of CSTRs, but with a very large investment cost, as theoretically a PFR performance is reached with an infinite series of CSTRs.[9] Another solution is the use of active mixers in tubular reactors, such as ultrasonic micromixers and pulse-

Special Issue: Giuseppe Storti Festschrift

Received: February 8, 2021
Revised: April 29, 2021
Accepted: April 29, 2021

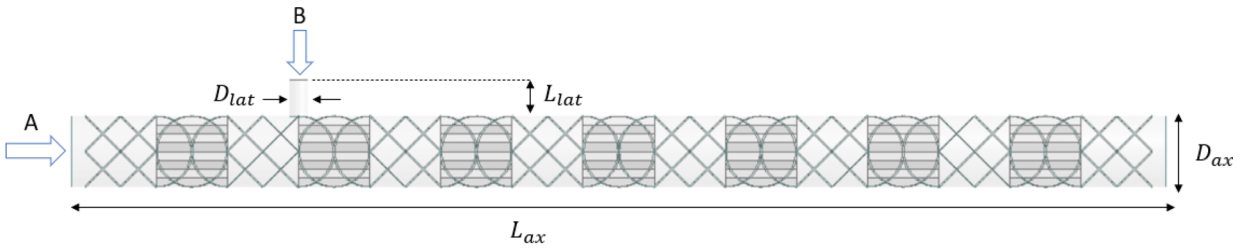

Figure 1. Side view of the reactor.

flow mixers. These solutions are efficient in mixing, but they are expensive and their operation is difficult, with high failure rates.[13]

A very promising alternative is the use of motionless mixers inside the tubular reactor. A chaotic flow is induced in the reactor and radial mixing is thus enhanced. Unlike active mixers, static mixers (SMs) have no moving parts, and the mechanical energy is obtained from the momentum of the flowing fluid, so they can achieve lower energy consumption and lower maintenance.[13,14] Because of their relatively simple and inexpensive nature, they are involved in a wide range of applications, such as in wastewater treatment, paper, food, pharmaceutical, petrochemical, and polymer industries.[14]

There are various types of static mixers, optimized for specific applications: considering laminar flows, one of the most efficient SMs is the Sulzer SMX, specifically designed to efficiently handle very diverse streams to be mixed, both in terms of flow rate and viscosities,[15] and complex rheological product behaviors.[16] These conditions are usually found, for example, in the polymer industry, where physical−chemical properties change widely during the reaction. Moreover SMXs have been demonstrated to be more efficient in mixing than other elements.[17,18]

The study of the properties influencing mixing inside SMs has already been examined, for example to observe the influence of viscosity inside Kenics static mixers,[19] the dependency on the Reynolds number in the laminar regime,[20] and the effect of mixing streams with different viscosities.[21] Nevertheless, to the authors knowledge, no comprehensive study is available on the mixing efficiency of the Sulzer SMX as well as the residence time distributions (RTD) attained in tubular reactors with side injections equipped with this type of SM. A side-injection tubular reactor is required when the goal is to reproduce in a continuous fashion a recipe usually carried out in semibatch reactors (SBR) when a kinetic-free approach is adopted.[22−24] This batch-to-continuous method does not require any information about the kinetic details of the reactions involved (i.e., no mechanism should be guessed, nor any kinetic constant should be found to apply this methodology). Consequently, it is possible to shift a discontinuous-reactor-based recipe to one run in a continuous tubular reactor with multiple side injections (or a series of tubular reactors with intermediate additions of reagents). The inlet axial stream has the composition of the fluid initially charged into the SBR, while the lateral feed composition is the same as one of the feed streams in the SBR. The lateral flow rates necessary to exactly reproduce the SBR performance in flow can be computed through this methodology initially as a continuous lateral injection[22,23] and then as discrete lateral injections.[24] The obtained reactor can be used for example when an additive (e.g., a coreactant, a catalyst, an inhibitor) should be mixed to the main stream through a lateral pipe, and generally the flow rate of such a lateral injection is smaller than that of the main (axial) stream, by at least an order of magnitude.[22−24] The aim of this work is to assess, using the Computational Fluid Dynamics, the mixing efficiency (in terms of mixing length) of the Sulzer SM for different fluid dynamic conditions in order to draw generalized considerations on the applicability of such SMs in reactors with lateral injections. A plot correlating the axial dispersion to the mixing length will be provided. Furthermore, the RTD of this reactor was determined to verify when a PF behavior is attained in the reactor. Consequently, the axial dispersion inside this reactor will be evaluated in order to be used with standard RTD models.

METHODS

Simulated Reactor. The modeled system consists of a tubular reactor equipped with 15 standard Sulzer SMXs with a length-to-diameter ratio of 1 and with crossed bars of thickness equal to 1 mm. The SMX mixing element consists of adjacent crossed bars rotated with an angle of 90° with respect to each other. Subsequent SM elements along the axis of the pipe are tangentially rotated by 90° with respect to the previous element. Each SMX element is composed of four couples of blades, and each couple of blades crosses to form a X in the channel: its aspect ratio, that is, the length of the SM to the reactor diameter ratio, is close to 1. The diameter of the pipe, D_{ax}, is equal to 5.08 cm. A lateral tube of diameter D_{lat} equal to 1.27 cm and length L_{lat} equal to 2.54 cm allows the injection of another stream. A side view of the reactor is reported in Figure 1 where the lateral injection is located, by way of example, at the end of the third SM element. This allows the flow field to be fully developed when the main stream (containing species A) mixes with the lateral stream (containing species B). An empty region of length equal to 1 cm diameter precedes and follows the series of SMXs. Consequently, the total length of the tube, L_{ax}, is equal to 78.2 cm. Table 1 summarizes the geometrical properties of the reactor used in the simulations, where D_{ax} is the diameter of the axial tube, D_{lat} is the diameter of the lateral tube, L_{ax} is the length of the axial tube and L_{lat} is the length of the lateral tube.

Table 1. Geometrical Properties of Reactor [cm]

D_{ax}	L_{ax}	D_{lat}	L_{lat}
5.08	78.2	1.27	2.54

The fed species A and B are characterized by a density ρ = 1000 kg m^{-3} and the simulations are performed at constant, uniform temperature. The viscosity of both the axial streams as reported in the results section, ranged between 5 × 10^{-4} and 10 pa·s. The massive flow rates of the two streams, $\dot{m}_A$ and $\dot{m}_B$

https://doi.org/10.1021/acs.iecr.1c00575
Ind. Eng. Chem. Res. XXXX, XXX, XXX−XXX

for the main and the lateral streams, respectively, define the flow rate ratio, $\dot{m}_A/\dot{m}_B$, and the mixture Reynolds number as

$$Re = \frac{4(\dot{m}_A + \dot{m}_B)}{\pi D \mu_{mix}} \quad (1)$$

where the mixture viscosity, $\mu_{mix} = \mu_A\omega_A + \mu_B\omega_B$, is computed from the mass fractions of A and B, $\omega_A = \dot{m}_A/(\dot{m}_A+\dot{m}_B)$ and $\omega_B = \dot{m}_B/(\dot{m}_A+\dot{m}_B)$.

Mixing Length. The mixing efficiency is estimated by means of the mixing length, L_{mix}, defined as the pipe length needed to achieve radial uniformity of composition after the position of the lateral injection. The degree of uniformity can be related to the coefficient of variation, COV, of the concentration of species B at a given axial position, x, in the reactor:[25]

$$COV(x) = \frac{\sqrt{(\overline{\omega_{B,x}^2} - \overline{\omega_{B,x}}^2)}}{\overline{\omega_{B,x}}} \quad (2)$$

where $\overline{\omega_{B,x}^2}$ is the mass-flow average of the squared mass fraction of B calculated at the axial position x and $\overline{\omega_{B,x}}$ is the mass-flow average of the mass fraction of B calculated at the axial position x. When COV $\leq$ 0.05, uniformity over the cross section of the reactor can be assumed. Thus, the mixing length corresponds to the distance from the lateral injection for which COV $\leq$ 0.05. COV values were computed at discrete positions along the axis of the reactor and intermediate values were obtained by linearly interpolating the logarithm of COV along the axial coordinate. The mixing length will be reported in terms of number of pipe diameters needed to achieve perfect mixing, L_{mix}/D.

Residence Time Distribution Analysis. To study the residence time inside the reactor, a step injection of a tracer (through the lateral channel) can be simulated.[9] A steady-state simulation is initially performed by mixing A and B. Afterward, a tracer species is injected from the lateral tube with a step change in the inlet composition. The tracer has the same properties of species B, and its mass fraction is changed from 0 to 0.01. The cumulative distribution function (CDF) is determined by measuring the mass-weighted-average of the mass fraction of the tracer at a given position in the reactor over the cross section. The RTD is found by time differentiation of the CDF.[9] This way, spatially resolved RTDs can be obtained along the axial coordinate of the reactor.

In particular, dimensionless RTDs are considered, that is, the normalized distribution of the dimensionless residence time, E_θ, will be used. The dimensionless time is defined as $\theta = t/\bar{t}$, where t is time and $\bar{t}$ is the mean residence time, which corresponds to the first moment of the distribution E_θ. The analytical solutions of the tanks-in-series model (TISM)[9] and the axial-dispersion model (ADM)[12] were used to observe whether the determined RTDs resemble those of a PFR (or a tubular reactor with low dispersion). In particular, the number of equivalent CSTRs in series, N_{CSTRs} (for the TISM), and the dispersion number, $\Theta = 1/Pe$ (for the ADM, where Pe is the Peclet number, defined as the ratio between the advective transport rate and the diffusive transport rate, $Pe = Lv/\mathcal{D}$, where L is the characteristic length, v is the flow velocity, and $\mathcal{D}$ is the mass diffusion coefficient), were determined to measure the similarity of the system to a PFR.

CFD Simulations. In this work, continuity, momentum, and species mass fraction transport equations were solved with the RANS approach by means of the Ansys Fluent 19.1 CFD software over an unstructured computational grid (mesh). The mesh is composed of tetrahedral cells (with refinement close to the walls), and a mesh independence analysis was performed to assess the minimum number of cells required. The test was performed by calculating the mixing length (steady-state simulation) in the reactor with four meshes of 2.6, 3.0, 6.0, and 13.0 million cells with a flow rate ratio $\dot{m}_A/\dot{m}_B = 10$, the lateral injection positioned at the end of the third mixing element, and $\mu_A = \mu_B = 10^{-3}$ pa·s. These simulations provided a mixing length of 4.58, 4.53, 4.44, and 4.44 diameters, respectively. Consequently, the mesh with 6.0 million cells was selected with a maximum cell size of 5 mm and a size of approximately 1 mm close to the reactor walls. Tests performed at higher Reynolds numbers confirmed the reliability of this mesh. A detail of the selected mesh close to the lateral injection is reported in Figure 2.

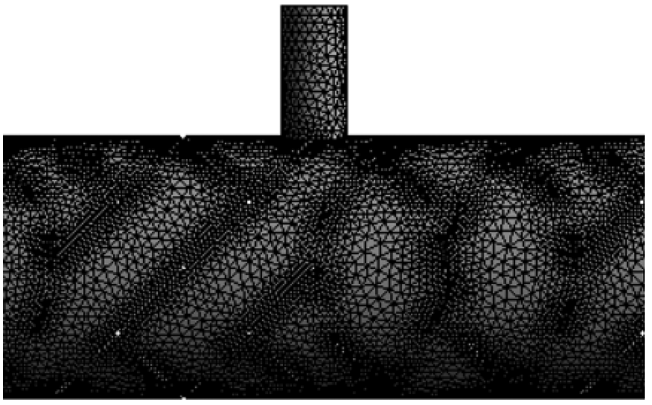

Figure 2. Detail of the selected mesh for the simulations.

The turbulence model used was the Shear−Stress Transport (SST) $k-\omega$ model, which was chosen thanks to its ability to model reliably fluids with different regimes ranging from laminar to turbulent.[26] The momentum and continuity equations were solved in a coupled fashion, with second-order schemes for space discretization. For transient simulations, a first-order-implicit time-stepping scheme was used. All the other solver parameters (e.g., turbulence model parameters, under-relaxation factors, and internal discretization parameters) were left to the default values. The boundary conditions for the walls of the reactor and for the SMs are nonslip walls with null species fluxes. The inlet boundary conditions (both axial and lateral) are set as mass flow inlet with assigned composition, while the outlet is set as a pressure outlet with null gauge pressure and backflow composition equal to the composition obtained when the axial and lateral streams are perfectly mixed. Convergence of the steady-state simulations (used in the mixing length analysis) was checked by visually observing low and constant residuals of the transport equations and by verifying the overall mass balance (i.e., mass conservation through the fluxes entering and exiting the reactor). Transient simulations (used for the RTD determination) were performed using a constant time stepping satisfying the Courant-Friedrichs-Lewy condition, that is, $Co = u\cdot\Delta t/h < 1$,[27] where Co is the Courant number, Δt the integration time step, and h the cell size. Through a time-

https://doi.org/10.1021/acs.iecr.1c00575
Ind. Eng. Chem. Res. XXXX, XXX, XXX−XXX

stepping-independence analysis, a time step of 0.07 s was selected and 25 iterations were allowed for each time step.

RESULTS AND DISCUSSION

To highlight the parameters influencing the mixing and residence time distribution of molecules inside the reactor, a simple standard case was chosen and selected parameters (viscosity, spatial velocity, mass flow rate ratio, number of lateral inlets) were varied one by one. The tables reported in the following sections will show only the changed parameters and if not differently specified the parameters will be assumed equal to the "standard" values. Table 2 shows the standard conditions adopted.

Table 2. Boundary Conditions and Fluid Properties for the Feeding Point Position Analysis

$\dot{m}_A$ [kg/s]	μ_A [Pa·s]	$\dot{m}_B$ [kg/s]	μ_B [Pa·s]	ρ_A [kg/(m^3·s)]	ρ_B [kg/(m^3·s)]	no. of inlets
10^{-2}	10^{-3}	10^{-3}	10^{-3}	10^{3}	10^{-3}	1

Mixing Analysis. A series of simulations were performed changing various properties both of the fluids and the reactor. For the sake of simplicity, all the chemical species in the reactor have the same density, equal to 1000 [kg/m^3].

More in detail, the parameters investigated were as follows:

- the lateral injection position
- the viscosity of species A, μ_A
- the spatial velocity inside the reactor, v
- the mass flow rate ratio, $\dot{m}_A/\dot{m}_B$
- the geometry of the reactor, as discussed in the following

Lateral Injection Position. Each static mixer is rotated by 90° in the tangential direction with respect to the previous element. Therefore, a series of simulations were performed to investigate the influence of the relative orientation between the lateral injection and the static mixer. Components A and B, having properties and flow rates reported in Table 2, were fed to the reactor. The lateral inlet was located at a distance from the axial inlet from 1 to 5 diameters.

We can see from the results reported in Figure 3, that the mixing lengths were almost equal when the lateral injection is located at a distance of 1, 3, and 5 diameters, while the ones computed with the inlet at 2 and 4 diameters were different. This means that the factor influencing the mixing is not the distance of the feeding point from the axial inlet, but rather the orientation of the static mixer with respect to the side injection.

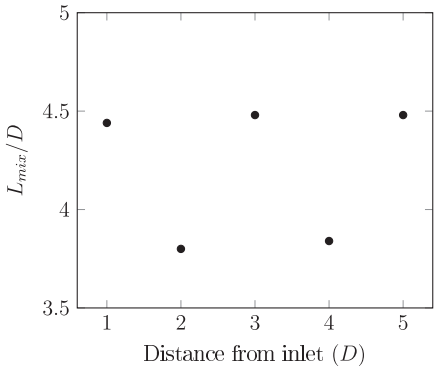

Figure 3. Mixing length as a function of the side injection position.

In particular, the inlet positioned at 2D and 4D is able to 'drag' more effectively the lateral flow, favoring the mixing with the axial flow.

Viscosity. In this set of simulations, the viscosity of the axial flow was changed as follows: $\mu_{A,1} = 1 \times 10^{-3}$ pa·s, $\mu_{A,2} = 1 \times 10^{-2}$ pa·s, $\mu_{A,3} = 1 \times 10^{-1}$ pa·s, $\mu_{A,4} = 1$ pa·s, $\mu_{A,5} = 10$ pa·s. B viscosity and mass flow rates were kept constant and equal to the standard case reported in Table 2.

The mixing length (Figure 4) rises with the viscosity and reaches a plateau for values of $\mu_A \geq 0.1$ pa·s). In particular, the mixing lengths do not exceed 10.8 diameters for the lateral injection located at 3D and 9.5 diameters for the lateral injection at 4D.

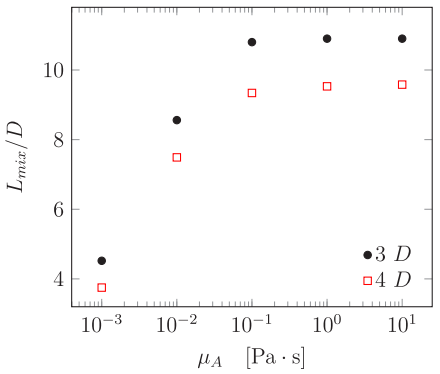

Figure 4. Mixing length as a function of A viscosity evaluated when the side injection is located at 3D or 4D from the inlet.

The different values obtained injecting the component B at a distance of 3 and 4 diameters from the inlet confirm the results discussed in the previous section. Moreover, the influence of the viscosity of species B was studied by simulating the mixing of fluids for which $\mu_B > \mu_A$. In more detail, the viscosity of the lateral flow was changed as follows: $\mu_{B,1} = 1 \times 10^{-2}$ pa·s, $\mu_{B,2} = 1 \times 10^{-1}$ pa·s, $\mu_{B,3} = 1$ pa·s, $\mu_{B,4} = 10$ pa·s, while the viscosity and mass flow rate of species A were kept constant and equal to the ones reported in Table 2. Results reported in Figure 5 show that the mixing length increases as the μ_B increases, but the maximum mixing lengths obtained are smaller than the ones reported in Figure 4. Moreover, as injecting at 4D is more efficient than injecting at 3D, from now on only 4D injections will be considered.

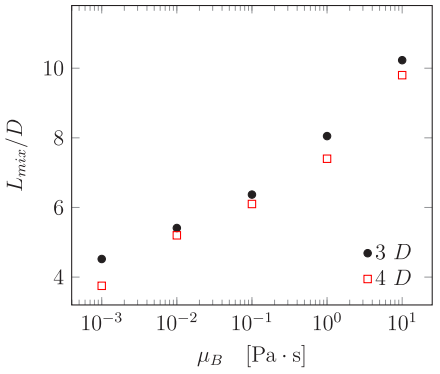

Figure 5. Mixing length as a function of B viscosity evaluated when the side injection is located at 3D or 4D from the inlet.

https://doi.org/10.1021/acs.iecr.1c00575
Ind. Eng. Chem. Res. XXXX, XXX, XXX−XXX

Spatial Velocity Variation. This set of simulations was focused on the effect of the spatial velocity on the mixing length by changing the value of the inlet mass flow rate of *A*.

To maintain the ratio between the inlet mass flow rates equal to 10, the lateral mass flow rate of *B* ($\dot{m}_B$) varies as well. The density and viscosity values are equal to the standard case reported in Table 2, while the mass flow rate values are summarized in Table 3.

Table 3. Boundary Conditions and Fluid Properties for the Spatial Velocity Analysis

$\dot{m}_A$[kg/s]	$\dot{m}_B$[kg/s]
10^{-2}	10^{-3}
5×10^{-3}	5×10^{-4}
2.5×10^{-3}	2.5×10^{-4}
1.25×10^{-3}	1.25×10^{-4}
2×10^{-2}	2×10^{-3}

Figure 6 shows the results obtained: we can see that the mixing is enhanced by higher velocities. This was expected,

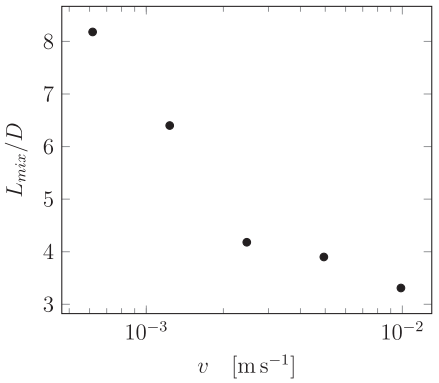

Figure 6. Mixing length as a function of spatial velocity.

since increasing the velocity means increasing the inertial forces impacting the static mixers blades.

Since the main parameter influencing the mixing is expected to be the Reynolds number, Figure 7 reports the mixing lengths as a function of the Re for the simulations performed by varying both the viscosity and the spatial velocity: we can see that all the mixing length values align on the same curve, therefore confirming the relevant role played by the ratio between inertial and viscosity forces.

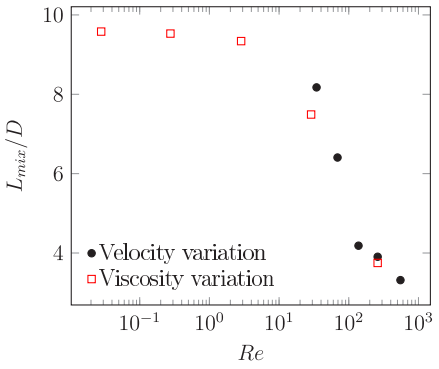

Figure 7. Mixing length as a function of Re.

Flow Rates Ratio. All the previous simulations were performed considering the ratio between the inlet mass flow rate of species A and the species B constant and equal to $\dot{m}_A/\dot{m}_B = 10$. In the following we investigate how a variation of this ratio affects the mixing length.

In particular, the mass flow rate ratio was modified acting on the mass flow rate of the component *B* (side injection), keeping constant (for each run) the mass flow rate of the component *A*. To also account for the influence of the *B* viscosity when the mass flow rate ratio is varied, some simulations with $\mu_B > \mu_A$ were performed, as reported in Table 4 and Table 5.

Table 4. Boundary Conditions and Fluid Properties for the Simulations with $\dot{m}_A/\dot{m}_B = 100$

$\dot{m}_A$ [kg/s]	μ_A [pa·s]	$\dot{m}_B$ [kg/s]	μ_B [pa·s]
2×10^{-2}	1	2×10^{-4}	10^{-3}
10^{-2}	10^{-1}	10^{-4}	10^{-3}
10^{-2}	10^{-2}	10^{-4}	10^{-3}
2.5×10^{-3}	10^{-3}	2.5×10^{-5}	10^{-3}
10^{-2}	10^{-3}	10^{-4}	10^{-3}
4×10^{-2}	5×10^{-4}	4×10^{-4}	10^{-3}
10^{-1}	10^{-3}	10^{-3}	10^{-1}
10^{-1}	10^{-3}	10^{-3}	1
10^{-1}	10^{-3}	10^{-3}	10

Table 5. Boundary Conditions and Fluid Properties for the Simulations with $\dot{m}_A/\dot{m}_B = 1$

$\dot{m}_A$ [kg/s]	μ_A [pa·s]	$\dot{m}_B$ [kg/s]	μ_B [pa·s]
2×10^{-2}	1	2×10^{-2}	10^{-3}
10^{-2}	10^{-1}	10^{-2}	10^{-3}
10^{-2}	10^{-2}	10^{-2}	10^{-3}
2.5×10^{-3}	10^{-3}	2.5×10^{-3}	10^{-3}
10^{-2}	10^{-3}	10^{-2}	10^{-3}
4×10^{-2}	5×10^{-4}	4×10^{-2}	10^{-3}
10^{-2}	10^{-2}	10^{-2}	10^{-1}
10^{-2}	10^{-2}	10^{-2}	1
10^{-2}	10^{-2}	10^{-2}	10

Figure 8 compares the mixing length obtained considering a mass flow rate ratio of 1, 10, and 100 in terms of *Re*. We can see that a ratio equal to 1 ensures a shorter mixing length, while up to the ratio equal to 10 a further increase of such a ratio does not affect significantly the mixing length obtained.

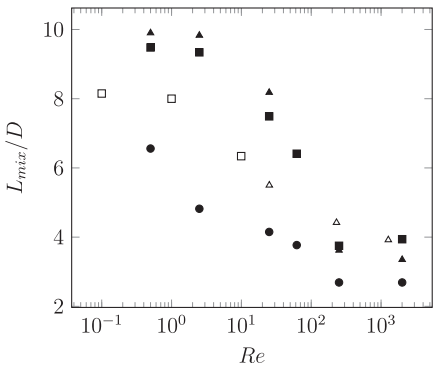

Figure 8. Mixing length as a function of *Re*: (●) $\dot{m}_A/\dot{m}_B = 1$; (■) $\dot{m}_A/\dot{m}_B = 10$; (▲) $\dot{m}_A/\dot{m}_B = 100$; (□) $\dot{m}_A/\dot{m}_B = 1$, $\mu_B > \mu_A$; (△) $\dot{m}_A/\dot{m}_B = 100$, $\mu_B > \mu_A$.

https://doi.org/10.1021/acs.iecr.1c00575
Ind. Eng. Chem. Res. XXXX, XXX, XXX−XXX

It should be noted that the results obtained with $\dot{m}_A/\dot{m}_B$ = 100 indicate that even very small lateral injections can be efficiently handled by the SM.

The simulations characterized by $\dot{m}_A/\dot{m}_B$ = 1 show appreciable differences with respect to that carried out with $\dot{m}_A/\dot{m}_B$ = 100 and $\dot{m}_A/\dot{m}_B$ = 10 for Re < 10^2, while for Re > 10^3 the mixing lengths are much more similar. This may be related to the fact that for higher values of *Re* the inertial forces are sufficiently high to lead to mixing length values as low as 3−4 diameters. Moreover, if $\mu_B > \mu_A$ the mixing lengths obtained are equal (for high *Re* values) or lower (for low *Re* values) than the ones obtained for $\mu_A > \mu_B$, confirming the results previously reported.

Inlet Geometry. The last parameter investigated was the injection geometry: a series of simulations were performed by varying the number of lateral injections on the same section. In particular, as shown in Figure 9, two opposite injection pipes and two couples of opposite injection pipes were considered.

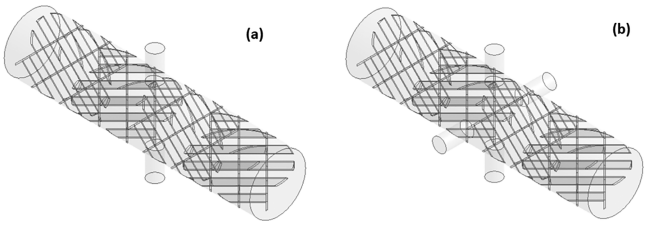

Figure 9. Reactor geometry with (a) two and (b) four lateral inlets.

Various *Re* were considered, varying both the viscosity and the spatial velocity inside the reactor, as summarized in Table 6, where $\dot{m}_B$ refers to the total flow injected through the two of four injection pipes. Thus, the flow entering each lateral tube is $\dot{m}_{B,i} = \dot{m}_B/n$, where *n* is the number of lateral tubes.

Table 6. Boundary Conditions and Fluid Properties for the Geometry Sensitivity Analysis

$\dot{m}_A$ [kg/s]	μ_A [pa·s]	$\dot{m}_B$ [kg/s]
2×10^{-2}	1	2×10^{-4}
10^{-2}	10^{-1}	10^{-4}
10^{-2}	10^{-2}	10^{-4}
2.5×10^{-3}	10^{-3}	2.5×10^{-5}
10^{-2}	10^{-3}	10^{-4}
4×10^{-2}	5×10^{-4}	4×10^{-4}

From the results reported in Figure 10 we can see that dividing the lateral injection among various inlets promotes a significantly lower mixing length, particularly for low values of *Re*.

Once more, the differences obtained become less and less significant increasing the Reynolds number, as for *Re* > 10^3 all the mixing lengths are approximately equal: starting from this value, the inertial forces lead to the minimum mixing length, and differences due to the number of injection pipes tend to vanish.

All the results discussed are summarized in Figure 11 as a function of *Re*. We note the following:

- In the "worst case" ($\dot{m}_A/\dot{m}_B$ = 100 and $\dot{m}_A/\dot{m}_B$ = 10 with a single lateral inlet) for values of *Re* having an order of magnitude of 10^1, a plateau is reached and the mixing length does not further increase; similarly, for values of *Re* with an order of magnitude of 10^3 a second plateau is reached and the mixing length does not further diminish. In other words, in these conditions the diagram can be roughly divided in three zones which may represent the laminar, transitional, and turbulent regime in a pipe equipped with Sulzer SMX static mixers.
- If the mass flow ratio between *A* and *B* is decreased or the number of lateral injections is increased, the mixing process is enhanced, leading to smaller mixing lengths.

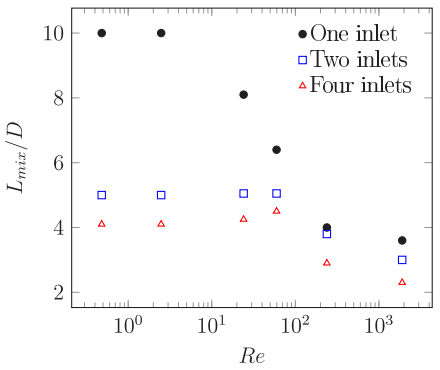

Figure 10. Mixing length as a function of *Re*.

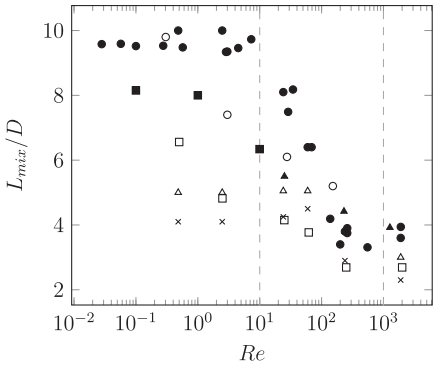

Figure 11. (●) $\dot{m}_A/\dot{m}_B \geq 10$, one inlet; (□) $\dot{m}_A/\dot{m}_B$ = 1, one inlet; (△) $\dot{m}_A/\dot{m}_B$ = 100, two inlets; (×) $\dot{m}_A/\dot{m}_B$ = 100, four inlets; (■) $\dot{m}_A/\dot{m}_B$ = 1, $\mu_B > \mu_A$, one inlet; (▲) $\dot{m}_A/\dot{m}_B$ = 100, $\mu_B > \mu_A$, one inlet; (○) $\dot{m}_A/\dot{m}_B$ = 10, $\mu_B > \mu_A$, one inlet; ($0 < Re < 10^1$) laminar region; ($10^1 < Re < 10^3$) transition region; ($Re > 10^3$) turbulent region.

The boundaries of the three zones identified on the diagram of Figure 11 (on the order of magnitude of $Re \cong 10^1$ and $Re \cong 10^3$) can be justified by looking at the ratio between the turbulent and laminar viscosity. The turbulent viscosity ratio, directly proportional to the turbulent Reynolds number, was computed for various *Re* and its values are reported in Figure 12. From the results, it is possible to see that the curve changes its slope in correspondence of $Re \cong 10^1$ and $Re \cong 10^3$, therefore roughly identifying the same three zones as in Figure 11. This result has been confirmed also by other authors.[28]

Residence Time Distribution Analysis. A series of simulations, using a First Order Implicit scheme, was performed to investigate the effect of the Reynolds number on the RTD. In particular, two points for each zone (laminar, transition, and turbulent) were selected as summarized in Table 7. Once the RTD curve was obtained, the reactor was modeled using both the tanks-in-series-model and the axial dispersion model.

Table 7 also reports the number of CSTRs in series and the inverse of the Peclet number that are able to reproduce the

https://doi.org/10.1021/acs.iecr.1c00575
Ind. Eng. Chem. Res. XXXX, XXX, XXX−XXX

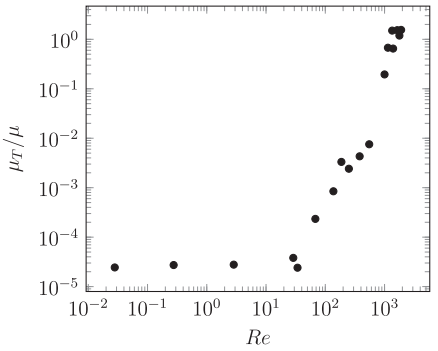

Figure 12. Turbulent viscosity ratio as a function of *Re*.

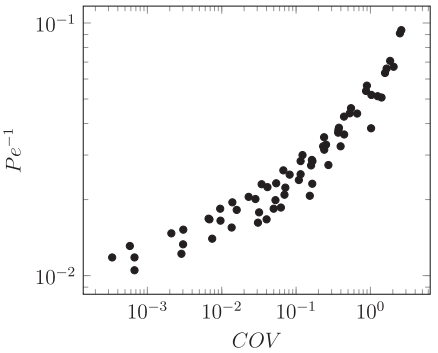

Figure 13. Pe^{-1} as a function of the coefficient of variation.

computed RTD, together with the estimated percentage of dead volume in the reactor.The results obtained with the axial-dispersion-model and tanks-in-series model are in perfect agreement with the ones reported by the Sulzer company.[29]

We can see that by increasing the Reynolds number the axial dispersion represented by Pe^{-1} decreases and the number of CSTRs able to approximate the reactor behavior increases. The fraction of dead volume is computed from eq 3:

$$V_{\text{dead}}[\%] = \frac{(\tau - \bar{t})\cdot Q}{V_{\text{reactor}}} \tag{3}$$

where τ is the ratio of the reactor volume to the total volumetric flow rate, Q is the volumetric flow rate, and V_{reactor} is the reactor volume.

For very low *Re* the dead volume fraction increases up to 10%: this may be caused by the increasing viscosity of the fluid, which creates a thicker region of low velocity near the walls, thus creating stagnant zones, as reported by other authors.[30]

It was noted that in the correspondence of the point in the reactor in which COV = 0.05 (where perfect mixing is assumed), the value of Pe^{-1} was almost the same for all the simulations performed. This implies that a graphic correlating the COV, which measures the dispersion along the radial coordinate, and the *Pe* which measures the dispersion along the axial coordinate, should exist, as reported in Figure 13.

We can see that Pe^{-1}(COV) has a monotonically increasing trend and when the flow is well mixed the axial dispersion is negligible and vice versa, that is, when COV $\leq$ 0.05 then $Pe^{-1} \leq 0.02$.

These RTD and mixing results can easily be applied together with a methodology available in the literature,[24] in which the transition from a SBR to a tubular reactor with multiple side injections was performed. The case study of the synthesis of amine/epoxy resins is considered: a recipe run in the SBR was reproduced with a series of 15 equal continuous tubular reactors (which were assumed to behave like PFRs), each having a single lateral injection and with a length equal to 87 diameters. For the selected case, *Re* ranged between 165 and 367 with flow rate ratios in the range 5−34 over the series of reactors. The fluid properties (ρ = 1060 [kg/m^3], $\mu = 10^{-3}$ [Pa·s]) were similar to the ones simulated in this work. From this study it follows that the PFR assumption used is reliable when Sulzer SMX are used, as good mixing of chemical species inside each reactor is achieved in approximately 4 diameters (as from Figure 11). This mixing length can be deemed small compared to the length of the reactor, thus the use of Sulzer SMX is very helpful in the application of batch-to-continuous methods when a PFR behavior is desired in the continuous reactor.

CONCLUSIONS

In this study, a series of analyses were performed to assess if a lateral injection tubular reactor equipped with Sulzer SMX static mixers can effectively ensure that the fluid motion is comparable to a plug flow reactor.

Results obtained confirm that such a reactor is effectively comparable to a plug flow reactor; even considering the laminar condition, a plug flow behavior is reached in less than 11 diameters in any flow condition. Finally, a plot correlating COV to Pe^{-1} and reported in Figure 13 was proposed, which allows a prediction of the *Pe* number, and then the axial dispersion of the reactor, through the COV values. These results were finally applied starting from previous literature results to a case study in the field of process intensification (transition of a SBR process into a continuous one).

Obviously, these conclusions hold true in the range of operating parameters investigated in this work. Investigations on the possible generalization of the evidenced behavior to other operating conditions (e.g., stream with different densities, multiphase streams, or reactive conditions) would extend the range of application of the aforementioned conclusions.

Table 7. Boundary Conditions, Fluid Properties, and Results of the RTD Analysis

$\dot{m}_A$ [kg/s]	μ_A [Pa·s]	$\dot{m}_B$ [kg/s]	μ_B [Pa·s]	Pe^{-1}	N_{CSTRs}	V_{dead} [%]
10^{-2}	10	10^{-3}	10^{-3}	1.99×10^{-2}	30	10
10^{-2}	1	10^{-3}	10^{-3}	1.84×10^{-2}	31	10
10^{-2}	10^{-1}	10^{-3}	10^{-3}	1.82×10^{-2}	33	4
10^{-2}	5×10^{-3}	10^{-3}	10^{-3}	1.67×10^{-2}	35	3
10^{-2}	5×10^{-4}	10^{-3}	5×10^{-3}	9.3×10^{-3}	70	0
4×10^{-2}	10^{-3}	4×10^{-3}	10^{-3}	7.7×10^{-3}	72	0

https://doi.org/10.1021/acs.iecr.1c00575
Ind. Eng. Chem. Res. XXXX, XXX, XXX−XXX

AUTHOR INFORMATION

Corresponding Author

Valentina Busini − *Department of Chemistry, Materials and Chemical Engineering "G. Natta", Politecnico di Milano, 20133 Milano, Italy;* orcid.org/0000-0001-5159-6279; Email: valentina.busini@polimi.it

Authors

Jody Albertazzi − *Department of Chemistry, Materials and Chemical Engineering "G. Natta", Politecnico di Milano, 20133 Milano, Italy*

Federico Florit − *Department of Chemistry, Materials and Chemical Engineering "G. Natta", Politecnico di Milano, 20133 Milano, Italy;* orcid.org/0000-0002-6484-4953

Renato Rota − *Department of Chemistry, Materials and Chemical Engineering "G. Natta", Politecnico di Milano, 20133 Milano, Italy;* orcid.org/0000-0002-3253-4424

Complete contact information is available at: https://pubs.acs.org/10.1021/acs.iecr.1c00575

Notes

The authors declare no competing financial interest.

REFERENCES

(1) Ilare, J.; Sponchioni, M.; Storti, G.; Moscatelli, D. From batch to continuous free-radical solution polymerization of acrylic acid using a stirred tank reactor. *Reaction Chemistry & Engineering* **2020**, *5*, 2081−2090.

(2) Durand, A.; Engell, S. Batch to Conti Transfer of Polymer Production Processes. *Macromol. React. Eng.* **2016**, *10*, 308−310.

(3) Kimura, H.; Tomatsu, K.; Saiki, H.; Arimitsu, K.; Ono, M.; Kawashima, H.; Iwata, R.; Nakanishi, I.; Ozeki, E.; Kuge, Y.; Saji, H. Continuous-Flow Synthesis of N-Succinimidyl 4-[18F] fluorobenzoate Using a Single Microfluidic Chip. *PLoS One* **2016**, *11*, e0159303.

(4) Benaglia, M.; Puglisi, A.; Porta, R.; Coccia, F. Organocatalysis chemistry in flow. *Current Organocatalysis* **2015**, *2*, 79−101.

(5) Asua, J. M. Challenges and Opportunities in Continuous Production of Emulsion Polymers: a Review. *Macromol. React. Eng.* **2016**, *10*, 311−323.

(6) Jas, G.; Kirschning, A. Continuous Flow Techniques in Organic Synthesis. *Chem. - Eur. J.* **2003**, *9*, 5708−5723.

(7) Diyoke, C.; Ngwaka, U. CFD Analysis of a Fully Developed Turbulent Flow in a Pipe with a Constriction and an Obstacle. *Intl. J. Eng. Res. Technol.* **2015**, *4*, 2278−0181.

(8) Ananthakrishnan, V.; Gill, W. N.; Allen, J. B. Laminar Dispersion in Capillaries: Part I. Mathematical Analysis. *AIChE J.* **1965**, *11*, 1063−1072.

(9) Levenspiel, O. *Chemical Reaction Engineering*, 3rd ed.; John Wiley & Sons, 1999.

(10) Nyande, W. B.; Thomas, M. K.; Lakerveld, R. CFD Analysis of a Kenics Static Mixer with a Low Pressure Drop under Laminar Flow Conditions. *Ind. Eng. Chem. Res.* **2021**, *60*, 5264−5277.

(11) Rojahn, P.; Hessel, V.; Nigam, K. D.P.; Schael, F. Applicability of the axial dispersion model to coiled flow inverters containing single liquid phase and segmented liquid-liquid flows. *Chem. Eng. Sci.* **2018**, *182*, 77−92.

(12) Florit, F.; Rota, R.; Jensen, K. F. Dispersion in coiled tubular reactors: A CFD and experimental analysis on the effect of pitch. *Chem. Eng. Sci.* **2021**, *233*, 116393.

(13) Klutz, S.; Kurt, S.; Kutup; Lobedann, M.; Kockmann, N. Narrow residence time distribution in tubular reactor concept for Reynolds number range of 10−100. *Chem. Eng. Res. Des.* **2015**, *95*, 22−23.

(14) Soman, S. S.; Madhuranthakam, C. M. R. Effects of internal geometry modifications on the dispersive and distributive mixing in static mixers. *Chem. Eng. Process.* **2017**, *122*, 31−43.

(15) Hirschberg, S.; Koubek, R.; Moser, F.; Schöck, F. An improvement of the Sulzer SMX^{TM}static mixer significantly reducing the pressure drop. *Chem. Eng. Res. Des.* **2009**, *87*, 524−532.

(16) Huai, L. Z.; Fasol, C.; Choplin, L. Residence time distribution of rheologically complex fluids passing through a Sulzer SMX Static Mixer. *Chem. Eng. Commun.* **1998**, *165*, 1−15.

(17) Rauline, D.; Le Blévec, J.-M.; Bousquet, J.; Tanguy, P. A Comparative Assessment of the Performance of the Kenics and SMX Static Mixers. *Chem. Eng. Res. Des.* **2000**, *78*, 389−396.

(18) Thakur, R.; Vial, C.; Nigam, K.; Nauman, E.; Djelveh, G. Static mixers in the process industries - a review. *Chem. Eng. Res. Des.* **2003**, *81*, 787−826.

(19) Belhout, C.; Bouzit, M.; Menacer, B.; Kamla, Y.; Ameur, H. Numerical Study of Viscous Fluid Flows in a Kenics Static Mixer. *Mechanika* **2020**, *26*, 206−211.

(20) Zalc, J. M.; Szalai, E. S.; Muzzio, F. J. Mixing Dynamics in the SMX Static Mixer as a Function of Injection Location and Flow Ratio. *Polym. Eng. Sci.* **2003**, *43*, 875−890.

(21) Regner, M.; Ostergren, K.; Trägårdh, C. Influence of Viscosity Ratio on the Mixing Process in a Static Mixer: Numerical Study. *Ind. Eng. Chem. Res.* **2008**, *47*, 3030−3036.

(22) Florit, F.; Busini, V.; Storti, G.; Rota, R. From semi-batch to continuous tubular reactors: A kinetics-free approach. *Chem. Eng. J.* **2018**, *354*, 1007−1017.

(23) Florit, F.; Busini, V.; Storti, G.; Rota, R. Kinetics-free transformation from non-isothermal discontinuous to continuous tubular reactors. *Chem. Eng. J.* **2019**, *373*, 792−802.

(24) Florit, F.; Busini, V.; Rota, R. Kinetics-free process intensification: From semi-batch to series of continuous chemical reactors. *Chem. Eng. Process.* **2020**, *154*, 108014.

(25) Montante, G.; Coroneo, M.; Paglianti, A. Blending of miscible liquids with different densities and viscosities in static mixers. *Chem. Eng. Sci.* **2016**, *141*, 250−260.

(26) *ANSYS Fluent Theory Guide*, release 19; ANSYS Inc., 2018; Vol. *1*.

(27) Rauter, M.; Hobe, L.; Mulligan, L.; Take, W.; Lovholt, F. Numerical simulation of impulse wave generation by idealized landslides with OpenFOAM. *Coastal Engineering* **2021**, *165*, 103815.

(28) Theron, F.; Le Sauze, N. Comparison between three static mixers for emulsification in turbulent flow. *Int. J. Multiphase Flow* **2011**, *37*, 488−500.

(29) Sulzer *Mixing and reaction technology*; version 15; 23.27.06.40; Sulzer, https://www.sulzer.com/-/media/files/products/static-mixers/mixing_and_reaction_technology_e_23270640.ashx?la=en.

(30) Cheng, S.; Zhang, L.; Wang, Y.; Zhang, X.; Chen, W. Residence time distribution of high viscosity fluids falling film flow down outside of industrial-scale vertical wavy wall: Experimental investigation and CFD prediction. *Chin. J. Chem. Eng.* **2019**, *27*, 1586−1594.

https://doi.org/10.1021/acs.iecr.1c00575
Ind. Eng. Chem. Res. XXXX, XXX, XXX−XXX